PLoS MEDICINE

Targeted Nanoparticles for Imaging Incipient Pancreatic Ductal Adenocarcinoma

Kimberly A. Kelly[1],*☉, Nabeel Bardeesy[2]☉, Rajesh Anbazhagan[1], Sushma Gurumurthy[2], Justin Berger[2], Herlen Alencar[1], Ronald A. DePinho[3], Umar Mahmood[1,4], Ralph Weissleder[1,2,4]

1 Center for Molecular Imaging Research, Massachusetts General Hospital and Harvard Medical School, Charlestown, Massachusetts, United States of America, 2 Massachusetts General Hospital Cancer Center, Massachusetts General Hospital and Harvard Medical School, Boston, Massachusetts, United States of America, 3 Center for Applied Cancer Science of the Belfer Institute for Innovative Cancer Science, Departments of Medical Oncology, Medicine and Genetics, Dana Farber Cancer Institute, Harvard Medical School, Boston, Massachusetts, United States of America, 4 Center for Systems Biology, Massachusetts General Hospital, Boston, Massachusetts, United States of America

Abbreviations: CLIO, crosslinked iron oxides; FACS, fluorescence-activated cell sorter; FITC, fluorescein isothiocyanate; H&E, hematoxylin–eosin; HUVEC, human umbilical vein endothelial cell; PanINs, pancreatic intraepithelial neoplasia; PDAC, pancreatic ductal adenocarcinoma; PTP, plectin-1 targeted peptide; PTP-NP, peptide conjugated nanoparticles; RITC, rhodamine isothiocyanate

* To whom correspondence should be addressed. E-mail: kkelly9@partners.org

☉ These authors contributed equally to this work.

ABSTRACT

Background

Pancreatic ductal adenocarcinoma (PDAC) carries an extremely poor prognosis, typically presenting with metastasis at the time of diagnosis and exhibiting profound resistance to existing therapies. The development of molecular markers and imaging probes for incipient PDAC would enable earlier detection and guide the development of interventive therapies. Here we sought to identify novel molecular markers and to test their potential as targeted imaging agents.

Methods and Findings

Here, a phage display approach was used in a mouse model of PDAC to screen for peptides that specifically bind to cell surface antigens on PDAC cells. These screens yielded a motif that distinguishes PDAC cells from normal pancreatic duct cells in vitro, which, upon proteomics analysis, identified plectin-1 as a novel biomarker of PDAC. To assess their utility for in vivo imaging, the plectin-1 targeted peptides (PTP) were conjugated to magnetofluorescent nanoparticles. In conjunction with intravital confocal microscopy and MRI, these nanoparticles enabled detection of small PDAC and precursor lesions in engineered mouse models.

Conclusions

Our approach exploited a well-defined model of PDAC, enabling rapid identification and validation of PTP. The developed specific imaging probe, along with the discovery of plectin-1 as a novel biomarker, may have clinical utility in the diagnosis and management of PDAC in humans.

The Editors' Summary of this article follows the references.

Introduction

Pancreatic ductal adenocarcinoma (PDAC) is the fourth leading cause of cancer deaths in the United States and shows a rapid clinical course, with a median survival of 6 mo and a 5-y survival rate of only 3% [1]. As chemotherapy and radiotherapy have only modest benefits, and surgery is only possible in 20% of patients, early detection that allows surgical resection offers the best hope for longer survival [2]. Indeed, the detection of PDAC or high-grade precursors in high-risk patient groups (e.g., hereditary cancer syndromes, chronic pancreatitis, and new-onset diabetes) represents a critical unmet need in the cancer diagnostic portfolio [3,4]. Additionally, tools to distinguish PDAC from benign cystic lesions frequently detected incidentally on cross-sectional imaging would be clinically useful by diminishing the need for invasive procedures. Currently, serum CA-19–9 is the only clinically used biomarker; however, it lacks the sensitivity needed to detect early-stage PDAC [5]. In addition, cross-sectional abdominal imaging has proven to be unreliable to detect early-stage PDAC in high-risk patients [6]. Therefore, considerable ongoing efforts aimed at identifying new PDAC detection biomarkers are currently being pursued using a variety of approaches including serum proteomics, expression profiling of tumor tissue, genetic analysis of pancreatic fluid, and methods using combinatorial chemistry [5,7–10].

There is a substantial challenge in studying the early molecular changes in PDAC because of the typical presentation of PDAC at advanced stage and the corresponding lack of suitable tissue specimens. Therefore, we elected to exploit a series of related genetically engineered mouse models of PDAC that harbor the signature gene mutations of the human disease, including Kras activation and deletion of the p53 or Ink4a/Arf tumor suppressors [11,12]. The tumors in these models exhibit the characteristic multistage histopathological progression (from precursor pancreatic intraepithelial neoplasis [PanINs] [13] to metastatic cancer) that defines PDAC in humans, providing tractable model systems for both biological and preclinical studies [11]. From these mouse models, we have been able to generate primary cell lines derived from emerging PDAC. These early-stage cancer cell lines, in conjunction with normal pancreatic ductal cells from wild-type mice [14], could facilitate screening for biomarkers and imaging agents using combinatorial chemistry-based approaches.

Early work to develop better diagnostic and therapeutic molecules has focused on the use of antibodies for tumor recognition and drug delivery [15,16]. However, antibody targeting in the case of molecular imaging often does not have ideal pharmacokinetics, has a limited target-to-background ratio, and furthermore has limited capacity for carrying magnetic resonance (MR)-detectable imaging agents unless extensively modified. Peptides are useful as targeting moieties with various high-throughput screening methods being utilized to select for ideal specificity, affinity, and pharmacokinetics. To their detriment as imaging agents, peptides generally have very short (<5 min) vascular half-lives and a lower affinity than their multivalent counterparts. The combination of multimodal nanoparticles with targeting peptides may circumvent some of these issues since they can be designed as platforms with optimized pharmacoki-

netics, allow multivalent peptide attachment, are small enough for targeting, and can be internalized into the cell resulting in signal amplification through intracellular trapping [17].

Here, we describe the use of peptide phage display and early passage PDAC cell lines isolated from the above mouse models to identify peptides that distinguish both human and murine PDAC cells from normal pancreatic ductal cells in vitro. In addition to the generation of imaging agents, the binding partners of the surface proteins identified in this approach represent a snapshot of the proteome in aberrant cells and may be useful for the delineation of the underlying signal transduction pathways important to disease progression.

Materials and Methods

Cell Culture

Primary mouse pancreatic ductal cells from wild-type mice were isolated and cultivated using published methods [14]. Early passage PDAC cell lines were isolated from tumors arising in Pdx1-Cre LSL-KrasG12D p53 L/L mice (designated Kras/p53$^{L/L}$) [11]. For the phage display experiments, PDAC cells were first grown in the primary duct cell media (F12 medium supplemented with 5 mg/ml D-glucose (Sigma), 0.1 mg/ml soybean trypsin inhibitor type I (Sigma), 5 ml/l insulin-transferrin-selenium (ITS+; BD Biosciences), 25 μg/ml bovine pituitary extract (BD Biosciences), 20 ng/ml epidermal growth factor (BD Biosciences), 5 nmol/l 3,3′,5-triiodo-L-thyronine (Sigma), 1 μmol/l dexamethasone (Sigma), 100 ng/ml cholera toxin (Sigma), 10 mmol/l nicotinamide (Sigma), 5% Nu-serum IV culture supplement (Collaborative Biomedical Products), and antibiotics (penicillin G 100 U/ml, streptomycin 100 μg/ml, amphotericin B 0.25 μg/ml; Gibco-BRL). Human PDAC cell lines (MNA, 8988, SW1990, MIA-PaCa-2, ASPC) were purchased from ATCC and cultured according to established protocols. NIH-3T3 cells (mouse fibroblasts) are purchased from ATCC. Murine heart endothelial cells (MHEC) were isolated from mice according to previously published protocols [18] and used after the second subculture. Human umbilical vein endothelial cells (HUVECs) were purchased from Clonetics and cultured according to the manufacturer's protocol.

Mouse Cohorts

Imaging studies were performed in Pdx1-Cre LSL-KrasG12D p53 L/+ (Kras/p53$^{L/+}$), Pdx1-Cre LSL-KrasG12D p16+/– (Kras/p16$^{+/-}$), Pdx1-Cre LSL-KrasG12D (Kras), and wild-type mice [11]. Breeding, genotyping, and analysis were performed as previously published [11,12]. All mice were housed in a pathogen-free environment at the Massachusetts General Hospital (MGH). The mice were handled in strict accord with good animal practice as defined by the Office of Laboratory Animal Welfare, and all animal work was done with Institutional Animal Care and Use Committee approval.

Phage Selection

Phage-positive selection and negative selection were achieved by incubating mouse PDAC cells isolated from the Kras/p53 mouse with phage (1×10^{11} PFU), which displayed a randomized linear 7–amino acid peptide library (phD7, New England Biolabs) for 1 h at 37 °C to allow time for phage to be

internalized into the PDAC cells. Screening for cell-internalizing phage affords a signal amplification by concentrating the imaging agent inside the cell, and in addition, the agent is not subject to k_{off} (off rate), further increasing the effective affinity [17]. To remove unbound phage and nonspecific binding phage, the cells were first washed with DPBS supplemented with 1% BSA and 0.05% Tween-20. Cell surface–bound phage were removed by washing with 0.1 M glycine (pH 2) for 8 min. Following a second glycine wash, the internalized phage were recovered by lysing the cells with 0.1% triethanolamine (Sigma) in PBS (pH 7.6) for 5 min at RT. The internalized phage pool was neutralized with 100 μl of 0.5 M Tris-HCl (pH 7). The counterselection was done by incubating the internalized phage pool with normal pancreatic cells for three 30-min cycles to effectively subtract all clones that bind to both normal pancreatic ductal cells and PDAC [19]. The internalized phage were amplified in *Escherichia coli*, titered, and subjected to three additional rounds for a total of four rounds of positive selection on the PDAC cells. From this selection, 30 clones were selected for sequencing and analyzed by ELISA (see below).

ELISA and Multidimensional Analysis

To facilitate choosing appropriate clones, we used ELISA and multidimensional analysis [20]. Briefly, PDAC and normal cells were grown to 100% confluence in a 96-well plate and incubated sequentially at 37 °C with the 30 phage clones (10^7 PFU, 1 h) in triplicate, washed with PBS containing 0.1% Tween-20, incubated with biotinylated anti-M13 antibody (1:40, 1 h), detected with streptavidin-HRP (1:500), developed with tetra-methyl-benzidine, and absorbance$_{650}$ was determined (Emax, Molecular Devices). Raw plate-reader outputs corresponding to PDAC or normal ductal cells were unpivoted to afford a denormalized table of values, and each well position was then associated with similar arrays of metadata labels. Values from each well were background subtracted using the median value of mock-treatment wells (wild-type phage) from each assay plate. Background-subtracted (B_{sub}) values for mock-treatment wells were accumulated across multiple assay plates to afford two mock-treatment distributions reflecting assay noise, one corresponding to PDAC cells and one corresponding to normal ductal cells, and trimmed according to Chauvenet's criterion as previously described (17). These mock-treatment distributions were used to normalize independently each value corresponding to a phage-treated well, affording Z-normalized (Z_{norm}) values for each well. All data formatting, manipulation, and normalization were implemented using Pipeline Pilot (Scitegic) and data visualizations (heat map) were prepared using DecisionSite (Spotfire).

Phage Labeling

For in vitro and in vivo validation experiments, phage were fluorochrome-labeled as previously described [21]. Briefly, ~1 × 10^{12} PFU of phage was suspended in 100 μl of 0.3 M NaHCO₃ (pH 8.6) containing either 1 mg/ml of fluorochrome-hydrosuccinimide ester (Cy5.5 or AF750) or 0.25 mg/ml of FITC (fluorescein isothiocyanate) or RITC (rhodamine isothiocyanate). The labeling reaction was allowed to continue in the dark at RT with gentle agitation. After 1 h, the reaction mixture was diluted to 1 ml in DPBS, and the labeled phage was purified by PEG precipitation (three times). The

fluorochrome-labeled phage was resuspended in 200 μl DPBS. Plaque-forming units were determined by titer analysis, and the concentration of the fluorochrome was determined spectrophotometrically (Varian Cary 11, Varian).

Phage Detection by Fluorescent Microscopy and Flow Cytometry

Mouse PDAC cells, human PDAC cells (MNA, 8988, SW1990, PaCa-2, ASPC), and normal human ductal cells were incubated with 1 μM (FITC) FITC-labeled phage clone 27 or unrelated phage clone (amino acid sequence SNLHPSD, negative control) for 1 h at 37 °C, washed three times with DPBS, then harvested by incubation with trypsin, centrifuged, and analyzed (10,000 cells/sample) by flow cytometry on a Beckton Dickinson FACSCalibur. All samples had a single narrow peak (e.g., Figure 1B). Mean fluorescence was plotted to describe relative uptake.

Ex Vivo Biopsy Specimens

For binding of PDAC-specific peptides to ex vivo mouse and human tissue sections ($n = 3$), biopsy specimens were snap frozen, embedded in OCT, cut into 5 μm sections, and then arrayed on slides. Slides were incubated with 1 μM of FITC-labeled phage clone 27 or FITC-labeled control phage (no insert) for 1 h at 37 °C, washed three times with PBS, fixed with 2% paraformaldehyde, and then visualized by fluorescence microscopy (Nikon Eclipse TE2000-S, Insight QE, 40× objective). Informed consent was not required for use of the human tissue specimens, as an exemption 4 applied (they were collected as part of routine patient clinical care). No identifying information was kept about the patients

Identification of Peptide Binding Partner

The phage were labeled with a photolinker (sulfo-SAED [sulfosuccinimidyl 2-(7-amino-4-methylcoumarin-3-acetamido) ethyl-1,3 dithiopropionate]; Pierce) and biotin tag using the same NHS chemistry used to conjugate fluorochromes to phage [21]. Two petri dishes (10 cm, Fisher Scientific) were plated with the target cell line and grown to confluency. One plate was incubated with 1 ml of the modified phage (roughly 10^{10} PFU/μl). As a negative control, the second plate was incubated with control (no insert) phage. Both plates were incubated in the dark at 4 °C for 1 h. The cells were then again washed several times with DPBS, placed on ice, and photolyzed 30 min using a 15-W 365-nm UV lamp (Spectroline), and lysed using 1% Triton X-100 in PBS with mammalian protease inhibitor cocktail added (Sigma). The cell lysates were incubated 1 h with 100 μl of Dynal Strepavidin beads (Invitrogen), which were preblocked with 5% BSA in PBS. The beads were washed twice with 1% Triton X-100 in 10× PBS, then incubated overnight at 4 °C with a buffer containing DTT to reverse the chemical crosslink and release the precipitated protein. Half of the eluate was transferred to a polyvinylidene fluoride (PVDF) membrane and probed with plectin-1 antibody (Santa Cruz Biotechnology). The other half of the eluate was loaded onto a SDS-PAGE gel (Biorad Criterion system) and stained using a mass spectroscopy–compatible silver stain (Invitrogen).

The band was then excised and sent for tryptic digest/mass spec analysis (Tufts Peptide Core Facility). Nanobore electrospray columns were constructed from 360-mm o.d., 75-mm i.d. fused silica capillary with the column tip tapered to a 15-
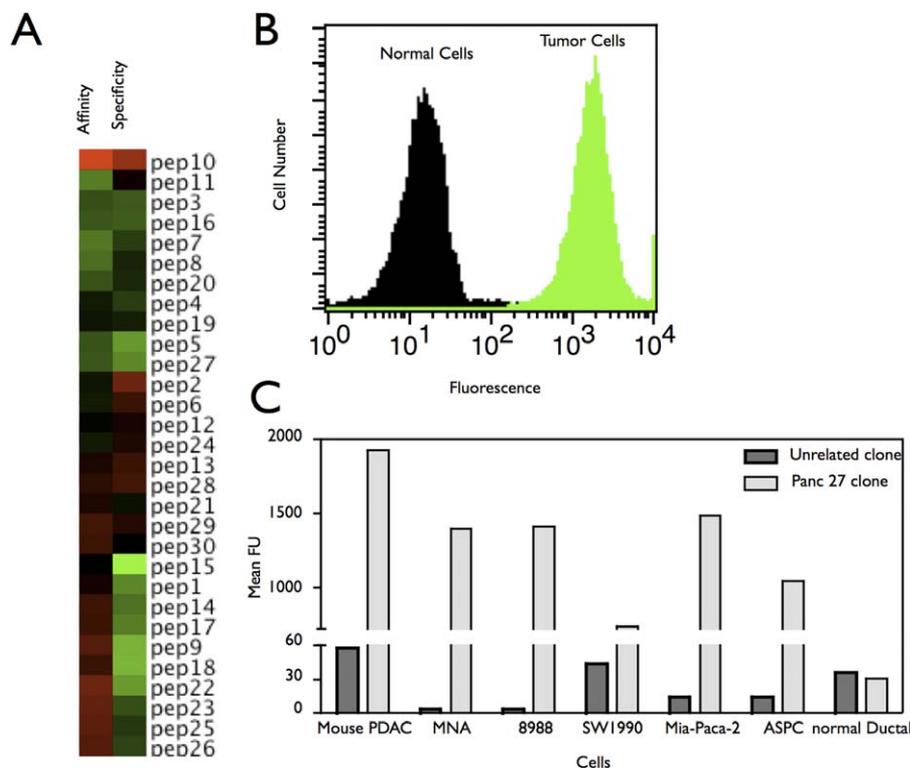
Figure 1. Isolation and Validation of PDAC-Specific Peptides

(A) After selection and subtraction, 30 individual phage clones were picked, amplified, and analyzed for affinity and specificity via ELISA. The heat map depicts affinity (mean absorbance values of indicated clones in ELISA assay) and specificity (ratio of clones' affinity to tumor cells versus normal ductal cells). Data are displayed in terms of higher rankings (green) to lower rankings (red).

(B) FITC-labeled clone 27 binds specifically to mouse PDAC cells. FITC-27 was incubated with PDAC or normal mouse ductal cells then analyzed via FACS.

(C) FITC-27 or FITC unrelated phage clone (negative control) were incubated with the indicated cells then analyzed via FACS. Data plotted are the mean fluorescence units obtained from FACS analysis.

doi:10.1371/journal.pmed.0050085.g001

mm opening. The columns were packed with 200-Å, 5-μm C18 beads (Michrom BioResources), a reverse-phase packing material, to a length of 10 cm. The flow through the column was split precolumn to achieve a flow rate of 350 nl/min. The mobile phase used for gradient elution consisted of (a) 0.3% acetic acid 99.7% water and (b) 0.3% acetic acid 99.7% acetonitrile. Tandem mass spectra (MS/MS) were acquired on a Thermo LTQ ion trap mass spectrometer (Thermo). Needle voltage was set at 3 kV. Ion signals above a predetermined threshold automatically triggered the instrument to switch from MS to MS/MS mode for generating fragmentation spectra. The MS/MS spectra were searched against the NCBI nonredundant protein sequence database using the SE-QUEST computer algorithm [9].

Verification of Panc 27 Binding to Plectin-1

Subcellular fractionation. PDAC, PaCa-2, 293T, HUVECs, and the normal ductal cells (mouse and human) were cultured overnight in two wells of a six-well plate. The cells were harvested via scraping with 500 μl of CLB (10 mM HEPES, 10 mM NaCl, 1 mM KH_2PO_4, 5 mM $NaHCO_3$, 1 mM $CaCl_2$, 0.5 mM $MgCl_2$) supplemented with 5 mM EDTA, 10 μg/ml aprotinin, 10 μg/ml leupeptin, and 1 μg/ml pepstatin. The harvested cells were allowed to swell for 5 min, homogenized 50 times then centrifuged at 7,500 rpm for 5 min. The pellet was suspended in 1 ml of TSE, 0.1% NP40, PI and homogenized for 30 min followed with centrifugation at

5,000 rpm for 5 min. The pellet was washed twice and suspended in 50 μl of TSE, 0.1% NP40, PI, leaving pure nuclei. The supernatant containing the cytosol with plasma membrane was centrifuged in a SW70 rotor at 70,000 rpm for 1 h. The pellet was resuspended and washed twice with CLB to remove contaminating cytoplasmic proteins. Protein concentration of each fraction was determined via BCA assay (PIERCE Biotechnology), and equal amounts of protein from each fraction were size-fractionated by SDS-PAGE. All fractions were analyzed for plectin-1 expression via Western blotting.

Competition experiments. Mouse PDAC cells were incubated with FITC-labeled phage clone 27 and either anti-plectin-1 antibody or vehicle for 1 h at 37 °C, washed, detached, then analyzed via flow cytometry (Becton Dickinson FACsCalibur).

Targeted nanoparticle synthesis. Plectin-1 targeted peptide (PTP) (amino acid sequence: KTLLPTP) or control peptide were synthesized by Tufts Peptide Core Facility with a GGSK(FITC)C linker for conjugation of the peptide to a model fluorescent nanoparticle (crosslinked iron oxides [CLIO]-Cy5.5). CLIO-Cy5.5 was synthesized in bulk using established procedures [22–25], and aliquots used for the synthesis of the various nanoparticle conjugates. Briefly, T-10 dextran was dissolved in water mixed with ferric chloride and degassed by nitrogen purging. Ferric chloride solution was added to the mixture and the pH brought to 10 with

ammonium hydroxide. The resulting particles were cross-linked with epichlorohydrin and ammonia to provide stability and amine groups for conjugation of fluorochromes and peptides. NHS-Cy5.5 was reacted with amino-CLIO in PBS overnight at 4 °C and purified by size exclusion chromatography. Determination of Cy5.5 loading onto CLIO was done by absorbance spectroscopy at 680 nm using unreacted CLIO as a reference (Figure S1A). CLIO-Cy5.5 had the following physical properties: (a) size 38.7 nm (Figure S1B), (b) relaxation time constants R1–21.1 and R2–62.6 mM/s, and (c) an average of 2.3 Cy5.5 per CLIO nanoparticle. To produce plectin-1 targeted or control nanoparticles, succinimidyl iodoacetic acid was reacted with CLIO-Cy5.5 for 15 min, purified by size exclusion chromatography, then reacted with peptidyl-cysteine for 1 h. Peptide-conjugated nanoparticles (PTP-NP) or controls (control-NP) were purified again using size exclusion chromatography and the ratio of peptides to nanoparticles was quantified at 497 nm by absorbance spectroscopy using unreacted CLIO as a reference (Figure S1C).

Intravital Laser Scanning Microscopy

The laser scanning microscope with far-red and near-infrared imaging capabilities (IV 100, Olympus) has been described in detail elsewhere [26]. During all imaging sessions, mice were anesthetized (2% isoflurane in 2 l/min O$_2$), and a small midline incision performed to expose the pancreas. As an in vivo screening approach, we have used phage as targeted nanoparticles for imaging by labeling the phage coat proteins with a near infrared fluorochrome [21,27]. The Cy5.5-labeled phage were injected IV 4 h prior to imaging for both the distribution and tumor imaging studies. SYTOX green was injected 10 min prior to imaging. Subsequent to imaging, tumors were removed for histological analysis. Serial frozen sections were hematoxylin–eosin (HE) stained and stained for the presence of M13 phage. For PTP-NP imaging, the agent was injected 24 h prior to IV 100 imaging. Angiosense (Visen Medical) was injected 10 min prior to imaging to visualize microvasculature. Images were acquired using appropriate triple excitation (561 nm for RITC, 633 nm for Cy5.5, and 748 nm for Angiosense-750). After fluorescence imaging, the pancreas was removed and embedded in degassed 1% low melting point agar in PBS to prevent susceptibility interfaces during subsequent MRI imaging.

Biodistribution

Mice were maintained on a nonfluorescent diet (Harlen-Teklad) for 3 d prior to imaging and received an intravenous injection of PTP-NP or control probe (15 mg Fe/kg body weight), coupled to Cy5.5 for fluorescent imaging, 24 h before biodistribution studies were carried out. Excised tissues were rinsed in PBS and imaged on the Siemens Bonsai system and Olympus OV100 system using Cy5.5 filters. Probe accumulation in tissues was compared to free probe, and biodistribution data are expressed as a percentage of injected dose. Fluorescence differences between the tissues were corrected by imaging tissues/organs from animals with no probe injected then subtracting this background from the total signal.

MRI

Pancreata imaged optically in vivo were then embedded, and ex vivo MRI studies performed to directly correlate intrapancreatic signal intensity changes with histology. Imaging of resected and agar-embedded specimen was performed using a Bruker 4.7T Pharmascan magnet, with a 38-mm diameter transmit-receive radiofrequency coil. Scout and localizer images were obtained, followed by high-resolution fast spin echo (FSE) and gradient echo sequences (GE). Specifically, for the T2 weighted FSE sequence, the following parameters were used: FOV 4.94 × 5.46 cm, matrix size of 512 × 512, slice thickness of 0.5 mm, RARE factor of 8, TE (effective) of 40 ms, TR 2811 ms, NEX of 50 for a total acquisition time of 2 h 29 min. For the T2* weighted GE sequence, the parameters were: FOV 3 × 3 cm, matrix size 512 × 512, slice thickness of 0.5 mm, TE of 6.8 ms, TR of 398 ms, flip angle of 30 degrees, NEX of 50, for a total acquisition time of 2 h 49 min. Fiducial markers were included to subsequently coregister high-resolution MRI datasets with histologic sections.

Histology and Immunohistochemistry

Pancreas and PDAC specimens were isolated and either fixed in 10% paraformaldehyde or frozen in OCT as previously described [11]. The histology and immunohistochemical analyses were done as previously described [11]. Serial frozen sections were stained with HE or for the presence of M13 (Amersham Biosciences) or plectin-1. Digital images were taken using a Nikon Eclipse E400 upright microscope (4× objective) equipped with an Insight color camera. Serial frozen sections were stained with HE or imaged via fluorescence microscopy for the presence of PTP-NP-Cy5.5 using a Nikon Eclipse 80i inverted microscope (20× objective) equipped with a 512 Photometrics Cascade CCD camera (Nikon).

Results

In Vitro Selection and Validation of PDAC-Specific Peptides

In this study, we made use of a genetically engineered mouse model of PDAC that closely recapitulates the histopathological, genomic, and molecular features of the human disease [11]. The Kras/p53$^{L/L}$ model [11] and wild-type controls served as a source of early passage PDAC cell lines and normal pancreatic ductal cells, respectively, for use in phage display selection and subtraction procedures to identify a pool of phage peptides specific for PDAC cells. Subsequent to selection procedures, we isolated 30 individual phage plaques and performed an ELISA to identify the most selective phage for PDAC cells. The results of two experiments performed in triplicate are presented in the heat map shown in Figure 1A and in the bar graph shown in Figure S2. The heat map depicts affinity and specificity. Of the 30 phage clones analyzed, 16 phage clones (53%) had specificity for PDAC cells. We sequenced the top seven clones on the basis of ELISA and multidimensional analysis. Clones 27 and 5 share identical peptide sequences (KTLLPTP) and demonstrated ideal affinity and specificity for the target PDAC cells [17,21]. To validate clone 27 (Figure 1B) in addition to clones 1 (SGVEFLH), 9 (SKKDTHH), 15 (TMAPSIK), 17 (TQHQVTA), and 22 (VNDRNVK) (unpublished data), we fluorescein labeled the phage coat proteins and quantified the extent of phage clone binding and specificity for mouse PDAC and normal ductal cells via flow cytometry. Clone 27
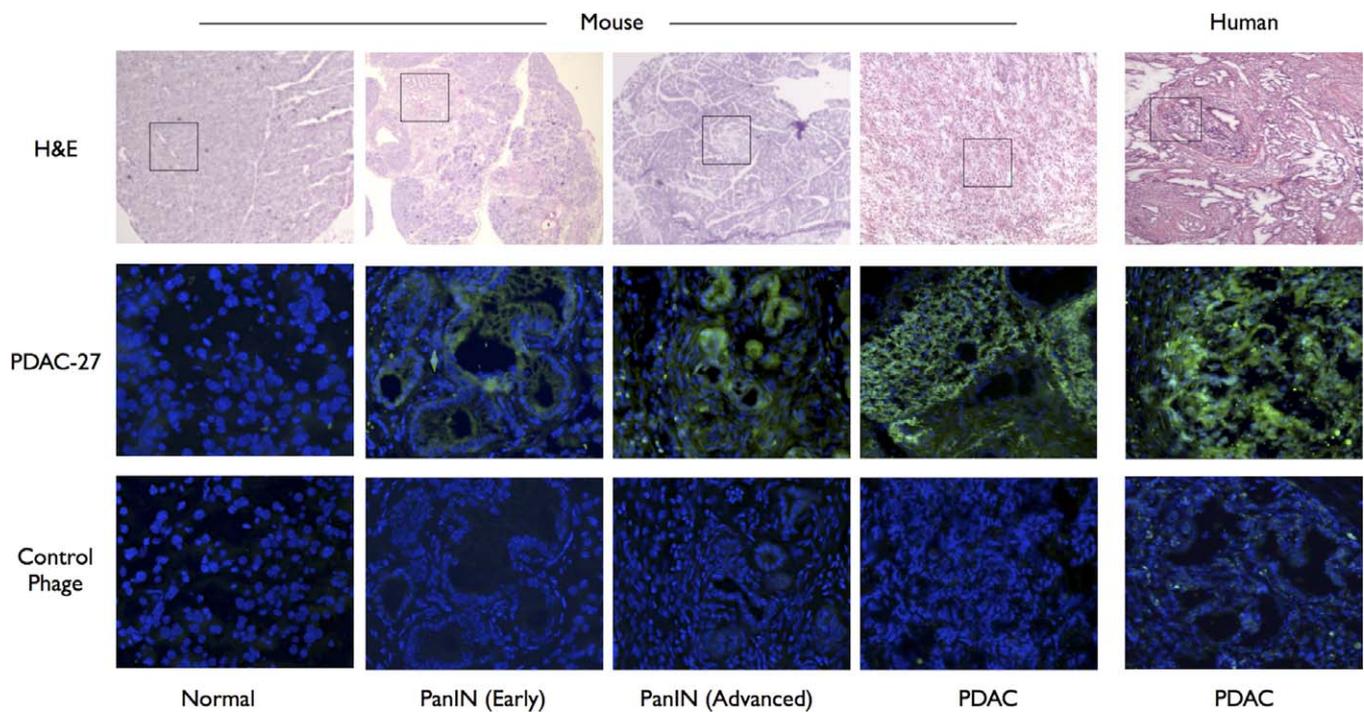
Figure 2. Clone 27 Detects Human PDAC

FITC-labeled clone 27 (PDAC-27) (middle row) or wild-type phage (no peptide insert; bottom row) were incubated with frozen sections of the indicated tissue. H&E staining of the same tissues is shown in the top row. Results shown are representative images.

doi:10.1371/journal.pmed.0050085.g002

was highly specific for mouse PDAC cells having a 112-fold specificity over normal ductal cells (Figure 1B). Phage clone 15 was second in affinity with the rest having nearly identical specificity (unpublished data). Together, these data demonstrate the effectiveness of our model-based phage screens for the identification and validation of phage clones with high affinity and specificity for mouse PDAC.

Specificity of Peptides for Human PDAC

We further validated the specificity of clone 27 by incubating FITC-27 or FITC-unrelated phage clone (negative control) with mouse PDAC cells, with five human PDAC cell lines, and with normal human ductal cells and then analyzing uptake via fluorescence-activated cell sorter (FACS). Clone 27 had an average specificity for PDAC cell lines of 141 (ratio of clone 27/unrelated clone mean fluorescence) when compared with unrelated phage. In addition, the two phage clones had nearly identical, weak binding to normal human ductal cells (specificity = 0.85).

We next determined the utility of the identified phage for the detection of mouse and human PDAC. Phage clone 27 labeled with fluorochrome was used as a probe to test binding to frozen sections of normal pancreas, pancreata containing focal PanINs, and pancreata with PDAC. While no binding was observed in wild-type mouse pancreata or in normal regions adjacent to lesions, prominent binding was observed in PanINs and PDAC lesions. Control phage failed to detect any lesions (Figure 2, bottom row). Phage clone 27, however, was able to specifically detect human PDAC, whereas control phage failed to stain human PDAC specimens (Figure 2, (far right)). These results demonstrate that the phage probes bind to evolving mouse and human PDAC, supporting the utility of

our models-based screening approach for the generation of candidate PDAC-specific diagnostic agents.

Tumor Localization of PDAC-Targeted Phage

Since phage clones 27 and 15 had the most favorable binding characteristics in vitro, wild-type animals or animals harboring PanINs or palpable pancreatic tumors were subsequently injected via tail vein with 1 nM of fluorescently labeled phage clone 27 and phage clone 15—alone or in combination—and then imaged via intravital confocal microscopy 4 h postinjection (Figure S3A). As a further control, tumor-bearing animals were injected with labeled phage containing a peptide isolated from an unrelated phage display screen (Figure S3B). Clone 27 illuminated PanINs and PDAC with a strong fluorescent signal, suggesting phage binding to tumors cells, whereas only a weak scattered signal was observed in the pancreas of wild-type mice (Figures 3A, 3B, and S3C). The fluorescent signal was virtually absent when control phage was injected into animals harboring emerging or advanced PDAC (Figure S3B). While clone 15 did localize to the pancreas, total signal was less than that of clone 27, prompting us to focus our efforts on clone 27. Clones 15 and 27 have distinctly different distributions within the pancreas and also different peptide sequences (Figure S3A), suggesting they target unique proteins. To further document the specificity of phage binding in vivo, pancreata from clone 27-injected animals were fixed and analyzed by immunohistochemistry using antibodies specific to phage coat proteins (Figure 3). In areas with PanINs or PDAC (black boxes in Figure 3B and 3C), there was strong uptake of phage whereas in regions of ductal metaplasia or normal pancreas (red boxes in Figure 3B and 3C) phage were undetectable. These studies
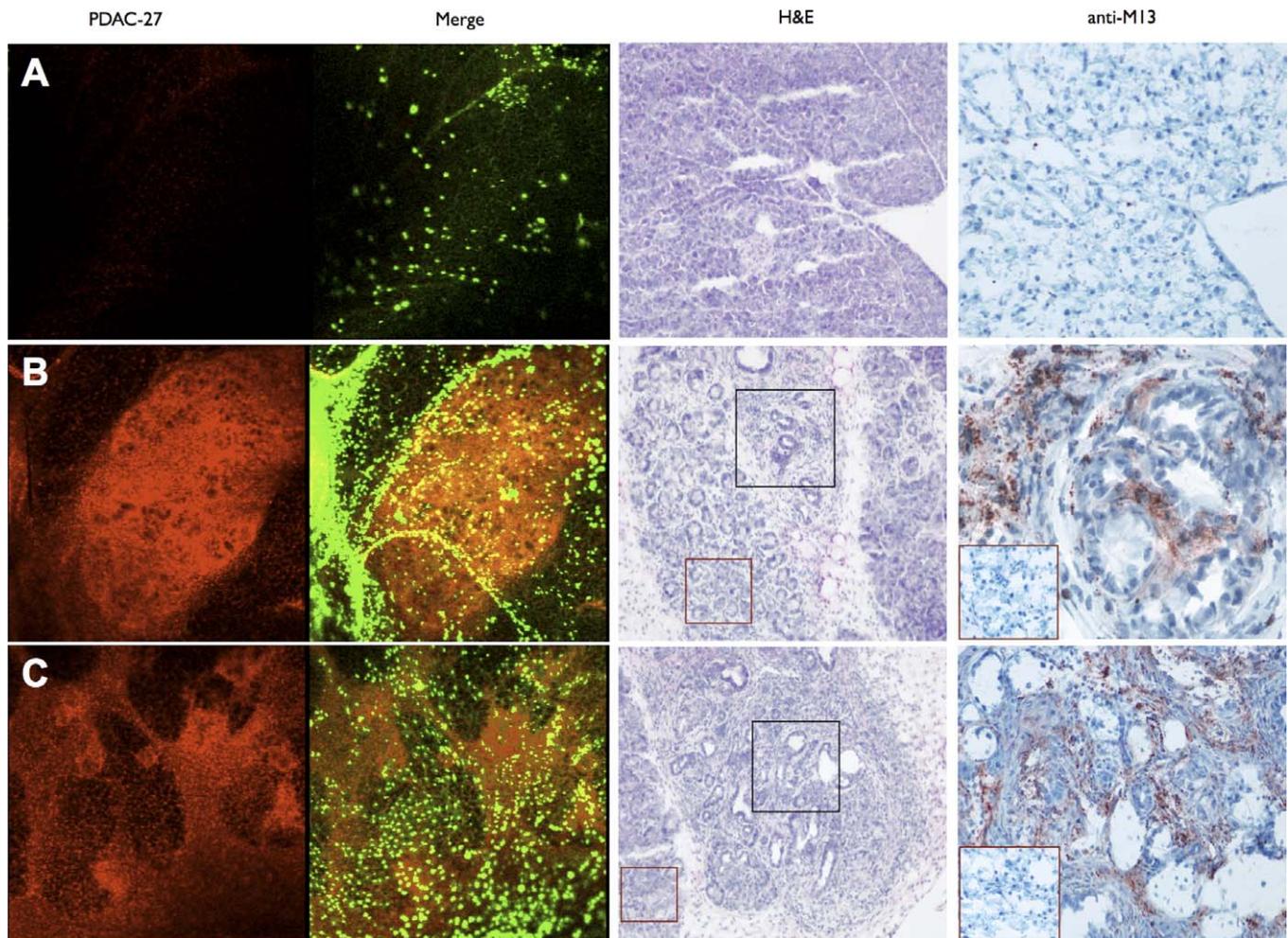
Figure 3. In Vivo Validation of Clone-27

(A) Wild type, (B) 29-wk-old Kras/p16$^{+/-}$, and (C) 12-wk-old Kras/p53$^{L/+}$ mice were injected with Cy5.5-labeled phage clone 27 (PDAC-27) and SYTOX green (nonspecific cell-labeling agent) then imaged via intravital confocal microscopy. Correlative Histology: Pancreata from intravital imaging experiments were embedded in OCT, frozen, and stained with HE or anti-M13 antibody. Black boxes correspond to regions of PanIN (B) or PDAC (C) and are magnified in the anti-M13 photomicrograph. Red boxes correspond to uninvolved adjacent regions (HE and inset in anti-M13 photomicrograph).
doi:10.1371/journal.pmed.0050085.g003

revealed that phage clone 27 was localized to PanINs and PDAC but was absent in normal pancreatic tissues or regions of ductal metaplasia, which are low-grade neoplasms or reactive lesions associated with pancreatic damage (Figure 3) [28].

Identification of Plectin-1 as the Binding Partner for Peptide 27

Since clone 27 showed exquisite specificity for human and mouse PDAC in vitro and in vivo, we sought to determine its binding partner. Using the phage as an affinity ligand, a unique 500-kDa band was identified in the mouse PDAC cell lysates via pull-down assay (Figure 4A, left). In addition, far-Western analysis of PDAC lysates with biotinylated phage as the probe identified a band of similar molecular weight that was not recognized by control phage (Figure 4A, right). Mass spectroscopic analysis of the isolated band revealed plectin-1, an intermediate filament and important crosslinking element of the cytoskeleton (Figure 4B) [29]. Western blot using lysates from the phage pulldown confirmed the presence of a band that cross-reacts with the plectin-1 antibody (Figure

4C). Plectin-1 is present in the membrane as well as the cytoplasm of both murine and human PDAC cells (Figure 4D). Normal mouse pancreatic ductal cells had low levels of plectin-1 expression, whereas normal human pancreatic ductal cells had plectin-1 expression in the cytoplasm and nucleus but not on the membrane (Figure 4D). HUVECs had very low levels of plectin-1 expression in the nucleus. As a control for plectin-1 expression, we used NIH-3T3 cells, which are known to have plectin-1 in the cytoplasm and nucleus but not on the cell surface [29]. As was expected, plectin-1 was absent from the membrane but present in the cytoplasmic and nuclear fractions of fibroblasts (Figure 4D). Immunohistochemical analysis of sections from normal, PanIN, or PDAC-harboring mice corroborated the Western analysis findings. Normal animals had scattered plectin-1 staining, whereas in PanINs and PDAC, plectin-1 was expressed in the lesions but not in the surrounding tissue (Figure 4E). The plectin-1 staining patterns were nearly identical to that observed by PDAC-targeted phage shown in Figure 3 (Figure 4E). Finally, in a competition experiment, coincubation of anti-plectin-1 antibody and FITC-labeled
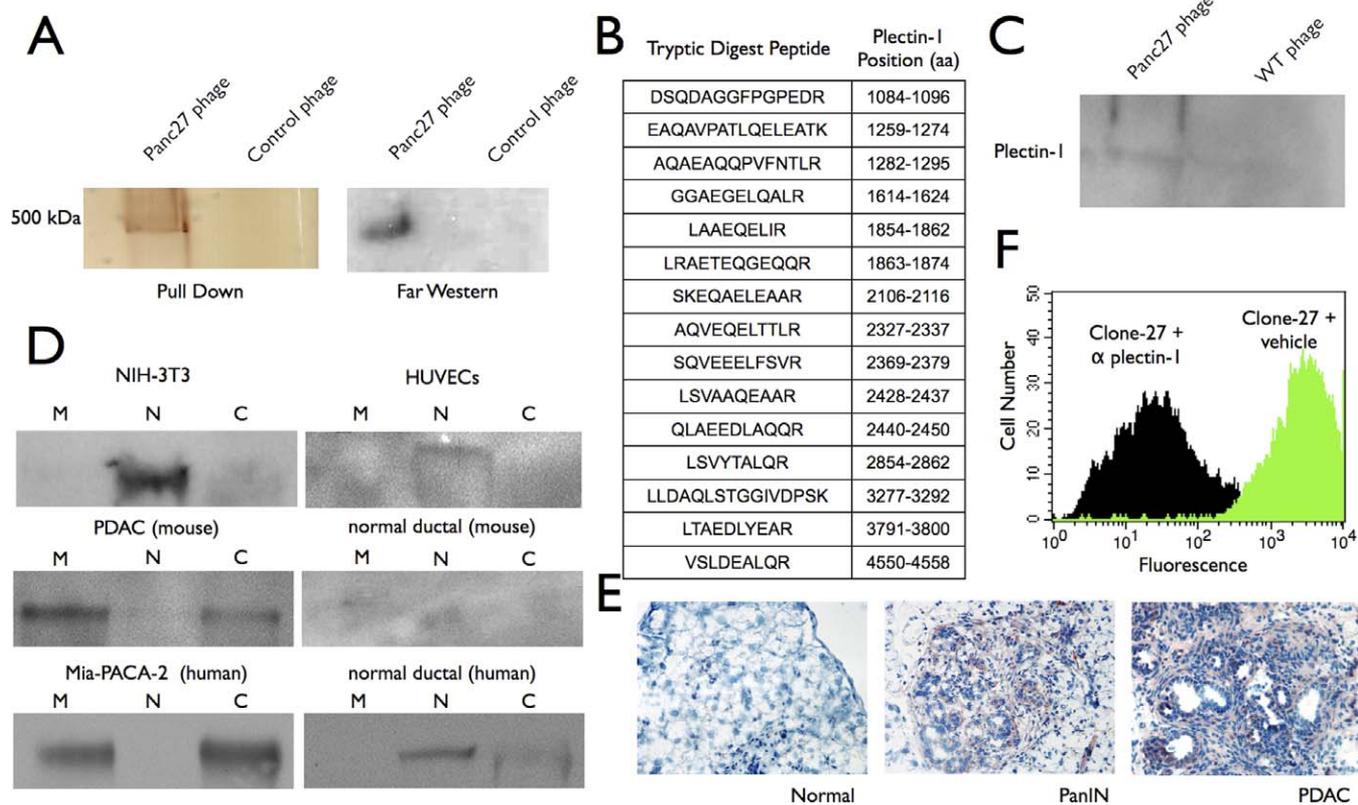
Figure 4. Identification and Validation of Plectin-1 Binding to Clone-27

Mouse PDAC cells were incubated with either sulfo-SAED and biotin-modified phage clone-27 or control phage, exposed to light, and lysates were incubated with streptavidin-coated beads.

(A) Precipitated protein was eluted with dithiothreitol (DTT) then run on an SDS-PAGE gel and silver stained (left). Far Western (right): PDAC lysates were loaded onto an SDS-PAGE gel then transferred and analyzed with clone-27 or control (no insert) biotinylated phage.

(B) A band corresponding to clone-27 affinity-purified protein from (A) was cut from the gel, digested with trypsin, and analyzed via mass spectroscopy.

(C) Affinity-purified protein from (A) was run on a SDS-PAGE gel, transferred to PVDF, and analyzed for the presence of plectin-1 with antibody to plectin-1.

(D) 293T cells, human umbilical vein endothelial cells (HUVECs), mouse PDAC cells, mouse normal duct cells, Paca-2 cells (human PDAC), and normal human duct cells were subcellularly fractionated, and the components probed for the presence of plectin-1.

(E) Pancreata from wild-type (left), 29-wk old Kras/p16$^{+/-}$ (center), and 12-wk old Kras/p53 (right) mice were embedded in OCT, frozen, and stained with anti-plectin-1 antibody.

(F) Competition experiment: mouse PDAC cells were incubated with FITC-labeled clone 27 and either plectin-1 antibody or vehicle then analyzed via FACS for the ability of clone 27 to bind.

doi:10.1371/journal.pmed.0050085.g004

phage clone 27 with PDAC cells resulted in 96.9% abrogation of binding (Figure 4F).

Development of Plectin-1 Targeted PDAC Imaging Agents

In order to develop a nonbiologic, synthetic imaging agent with translational potential, we chemically synthesized and attached PTP to a magnetofluorescent nanoparticle (PTP-NP) (schematic, Figure 5A). The resultant MRI/optically detectable agent was tested in 9-wk-old Kras/p53$^{L/+}$ mice. At that age, these mice do not exhibit outward signs of illness but typically harbor small, focal PDAC, as well as regions of normal pancreas, ductal metaplasia, and fibrosis. Twenty-four hours after IV administration of the targeted nanoparticle, intravital confocal microscopy detected discrete areas of fluorescence in the abdominal region of these mice, suggestive of agent uptake (Figure 5B, left). The agent was specifically present in the tumor tissue as a vasculature agent administered 10 min before injection failed to colocalize (Figure 5B, right). The in vivo fluorescence correlated with surface reflectance imaging of the excised pancreas where discrete

foci of signal were found (Figure 5C). In contrast, control-NP failed to highlight any regions of the pancreas (Figure 5B, left), although these tumors were similarly vascularized (Figure 5B, right). Biodistribution studies revealed specific uptake in tumors with minimal uptake in muscle or skin, two tissues with reported plectin-1 expression (Figure 5D). In addition, tumor uptake relative to normal pancreas was 10.1-fold higher. Similarly, MRI showed a reduction in magnetic resonance (MR) signal indicative of agent presence in focal regions of the pancreas (Figure 6A). From the biodistribution data, 3.13%-injected dose of material was present in the tumors. Using previously established thresholds for direct MRI sensitivity of 10 ng of Fe/g of tissue [30], we calculate that the results are 20-fold over the threshold of detection. In addition, it is likely that today's sensitivity is higher than what was previously published given available motion correction and multi-echo chemical sequences. Histological analysis confirmed that the loss of signal associated with PTP-NP uptake was primarily in regions of PDAC but not in normal regions or regions of ductal metaplasia (Figure 6B). Fluo-
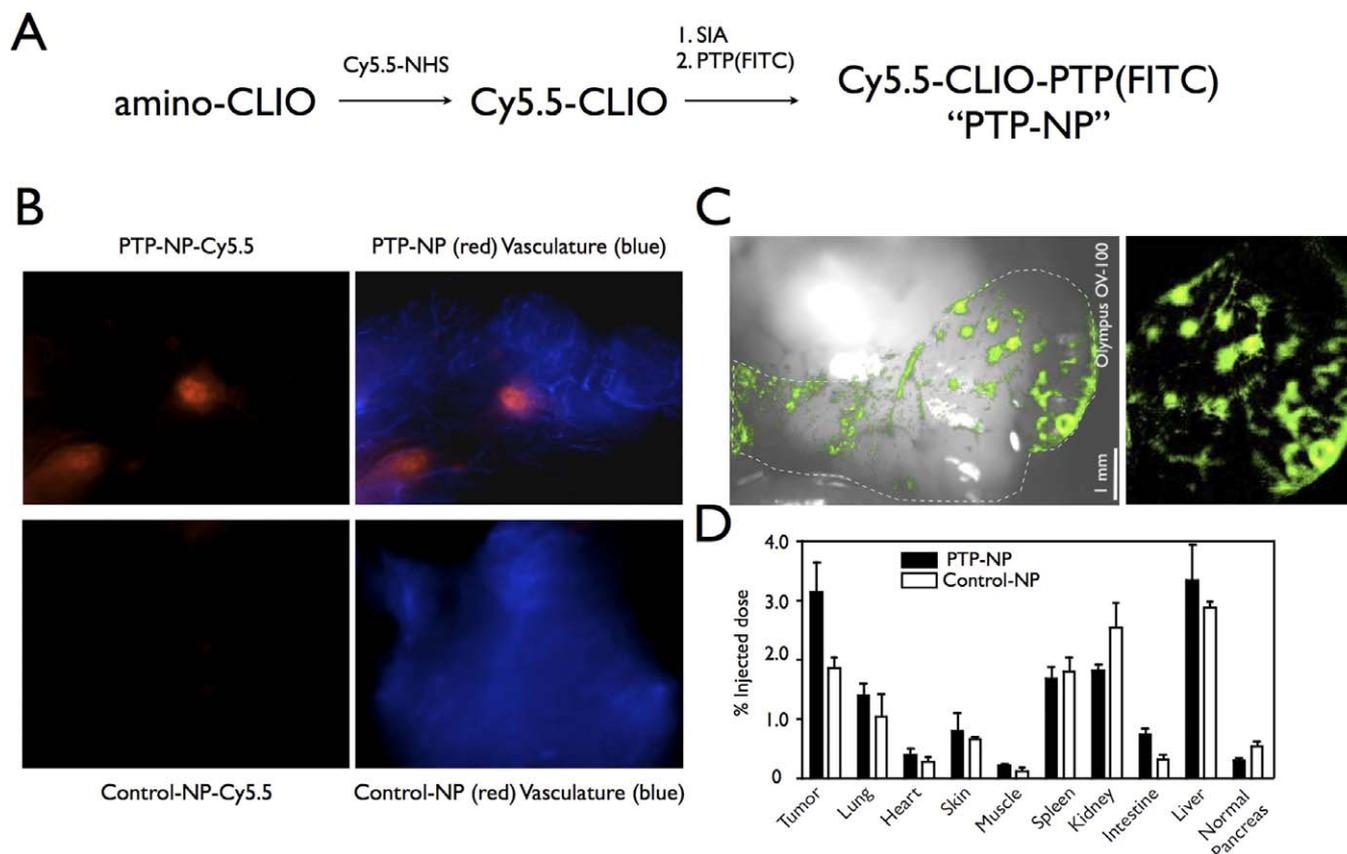
Figure 5. Fluorescence Imaging of PDAC Using PTP-NP or Control-NP

(A) Schematic of conjugation of PTP to NP. Control-NP is synthesized the same way with substitution of control peptide for PTP.
(B) Intravital confocal microscopy of early pancreatic lesions imaged using PTP-NP (red, top) or control-NP (red, bottom) and AF750-labeled bloodpool agent (blue).
(C) Low-magnification view of pancreatic fluorescence shows distribution of PTP-NP in distinct areas of the pancreas. White light overlay provides anatomic correlation (left). Dotted line outlines the pancreas.
(D) Biodistribution of PTP-NP and control-NP.
doi:10.1371/journal.pmed.0050085.g005

rescence microscopy of the sections demonstrated PTP-NP accumulation in areas of PDAC (Figure 6C, left) but not in areas of normal pancreas (Figure 6C, right).

Discussion

Using a phage display screen and exploiting the experimental merits of a refined genetically engineered mouse model of PDAC, we successfully generated a multimodal nanoparticle-based targeted imaging agent, PTP-NP, that allows imaging of PDAC in the background of normal, mucinous, and ductal metaplasia of the pancreas. The imaging agent has potential use for both MRI and endoscopy in high-risk patients. Important issues in the development of improved diagnostics for PDAC include the need to distinguish pancreatic neoplasia from regions of pancreatic damage and the need for methods that identify earlier stages of tumor progression [31]. The imaging probes identified in this study home to the neoplasm while showing no appreciable colocalization with adjacent areas or acinar-ductal metaplasia. This specificity could be used to possibly reduce "false-positives" in diagnostic tests. Further, these new imaging probes bind to PanINs as well as to advanced cancers. The capacity to detect such premalignant lesions

could enable the development of new approaches in the management of this disease. Although liver and kidney uptake is high, the tomographic imaging techniques that would be used with this probe (i.e., MRI, single photon emission computed tomography [SPECT]/CT, or optical) would allow the resolution of the pancreas in the context of both organs.

In addition to the development of novel molecularly targeted imaging agents, phage display screening and modified immunoprecipitation permitted the identification of membrane-localized plectin-1 as a potential new biomarker for PDAC. Differential protein processing and/or trafficking, identified using proteomic approaches, represents a potential class of biomarkers that would be missed if looking at cDNA expression data only or using whole-cell proteomics methods. For example, the binding partner of clone 15 identified from this screen represents an additional biomarker that may shed light on aberrant molecular pathways contributing to PDAC pathogenesis.

Plectin-1 is a high molecular weight protein (500 kDa) that links intermediate filaments to microtubules and microfilaments and also anchors the cytoskeleton, the plasma, and nuclear membranes (reviewed in [29]). We have shown that plectin-1 levels are low in normal pancreatic ductal cells, but
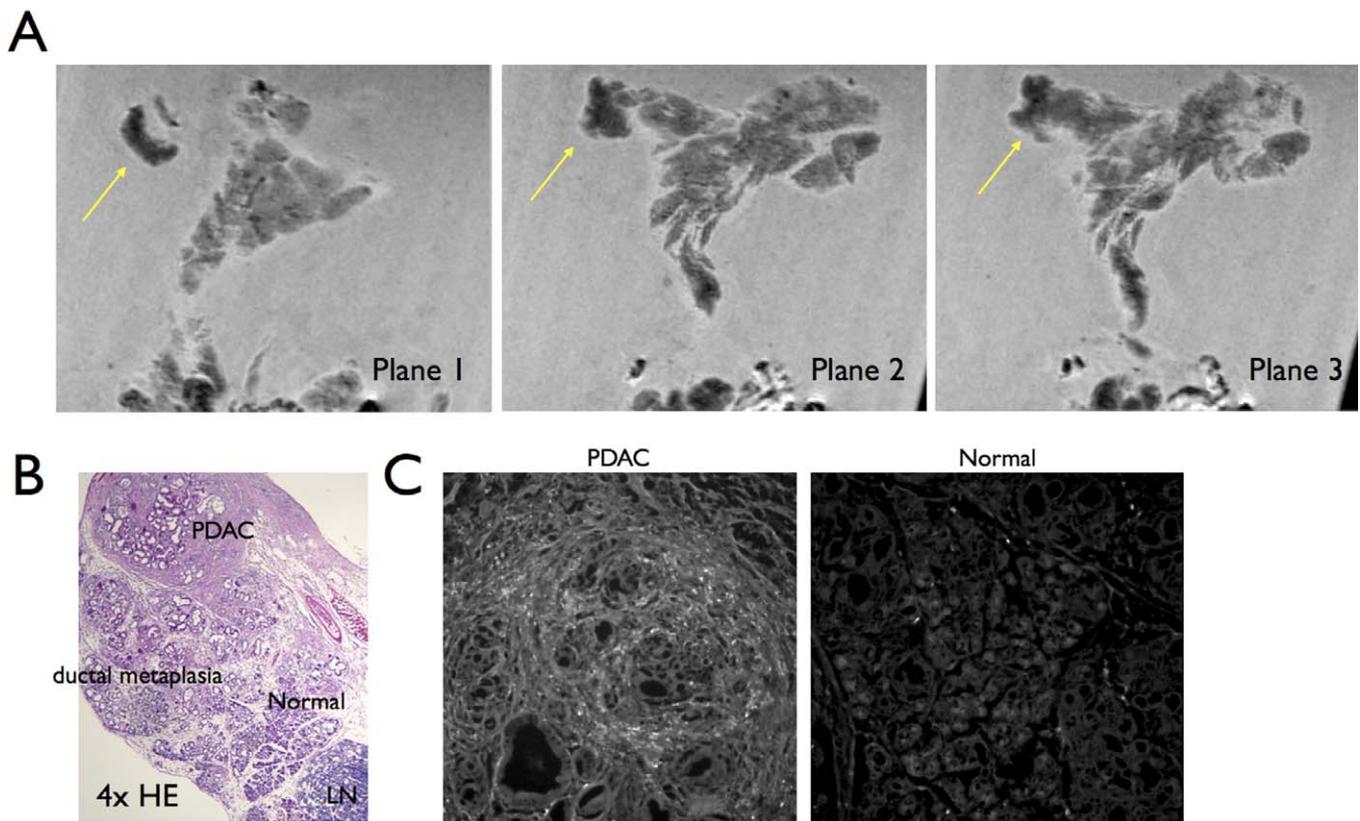
Figure 6. MRI and Correlative Histology

(A and B) Three adjacent slices (A) from an ex vivo MRI of the pancreas from a 9-wk-old Kras/p53$^{L/+}$ mouse demonstrates focal nanoparticle uptake (one example, yellow arrow), which corresponds to tumor seen on correlated HE sections (B), but not to regions of ductal metaplasia or normal pancreas (labeled).

(C) Fluorescence microscopy of adjacent sections demonstrate uptake of Cy5.5-labeled PTP-NP in regions of tumor (left) but not in adjacent tissue (right).

doi:10.1371/journal.pmed.0050085.g006

its expression is upregulated in PanINs and remains elevated in PDAC. Perhaps more importantly, plectin-1 exhibits distinct cytoplasmic and nuclear localization in normal fibroblasts, whereas an aberrant expression on the cell membrane is observed in PDAC. Studying the mechanisms of protein upregulation, differential trafficking, and whether plectin-1 contributes to disease progression are important future experiments. Notable in this regard, recent publications illustrate that plectin-1 can be recruited to the membrane during epithelial cell transformation [32]. Altered subcellular localization of plectin-1 is also observed in the autoimmune condition, paraneoplastic pemphigus, and in the associated lymphoproliferative neoplasm, Castleman disease [33]. Plectin-1 has a number of important roles in signal transduction, influencing Rho activity [34], and serving as a scaffold for proteins involved in protein kinase C (PKC) [35] and AMP-activated protein kinase signaling pathways [36]. Thus, plectin-1 in PDAC may have an impact on signaling pathways that regulate cell migration, polarity, and energy metabolism.

Noninvasive imaging has particular applications in high-risk groups—hereditary PDAC kindreds and new-onset diabetes patients—who are currently targets of screening for pancreatic cancer. Despite the increased risk in these individuals, the incidence of pancreatic cancer will only be ~0.4%–0.6% [37], hence surgery, which carries substantial morbidity and mortality, is not typically carried out prophylactically. Traditional imaging such as CT scan or MRI often do not detect PDAC lesions until they have reached a size at which many tumors have already metastasized—rendering surgery ineffective. There is, consequently, a considerable need for a new imaging modality that would accurately identify the presence of PDAC at an earlier point in its evolution—when surgery is effective. Other settings for noninvasive imaging of incipient cancers include patients with cystic neoplasms: intraductal papillary mucinous neoplasms (IPMN) and mucinous cystic neoplasms (MCN). These tumors are often benign, however a subset progress to PDAC. Furthermore, there may be utility for these approaches in postsurgical screening for recurrence and screening prior to surgery to determine exact tumor extension more accurately. Finally, we envision that the approach could be clinically valuable in differential diagnosis, i.e., patients presenting with pancreatitis, jaundice, or upper abdominal pain. In screening of high-risk groups, it will be important to be able to distinguish low-grade PanINs, which are present in many healthy individuals, from high-grade PanINs and carcinoma in situ. The ideal probes would recognize lesions of PanIN-3 and higher since these are thought to have very high potential for progressing to invasive PDAC. Further work will be required to define whether the plectin-1 targeted nanoparticles discriminate between low-grade PanINs and high-

grade PanINs. Translational studies can be conducted in patients undergoing resection; the rapid homing of the agent to tumors and subsequent clearance from the body makes this technically feasible.

Genetically engineered mouse models of human cancers effectively recapitulate many of the molecular, biological, and clinical features of the human disease [11,12]. Recent genomics studies of mouse and human cancers have established that cross-species analysis can serve as an effective filter in identifying recurrent alterations [38,39]. Our studies here show that the utility of such mouse models extends to the development of molecularly targeted imaging agents. We identified conserved markers of early disease in screens that took advantage of mouse cell lines derived from the early stages of cancer development and primary pancreatic ductal cells. Furthermore, the known kinetics of tumor progression of our mouse model facilitated testing of the imaging probes at defined stages of tumorigenesis. The approaches described here may be broadly applicable to the discovery of cancer biomarkers predictive of disease stage, prognosis, or presence of specific genetic alterations.

Supporting Information

Figure S1. Characterization of Nanoparticles

(A) CLIO-Cy5.5 absorbance spectroscopy used for quantitation of number of Cy5.5/nanoparticle.
(B) Size distribution of CLIO via light scattering.
(C) Absorbance spectroscopy of PTP-NP-Cy5.5 used to quantitate the number of peptides/nanoparticle. Notice background absorbance from nanoparticle below 500 nm, whose contribution is subtracted via reference to unreacted CLIO.

Found at doi:10.1371/journal.pmed.0050085.sg001 (287 KB TIF).

Figure S2. Phage Clone Validation Via ELISA

After selection and subtraction, 30 individual phage clones were picked, amplified, and analyzed for affinity and specificity via ELISA.

Found at doi:10.1371/journal.pmed.0050085.sg002 (708 KB TIF).

Figure S3. In Vivo Imaging with Phage Clones 15 and 27

(A) Cy5.5-labeled phage clone 27 and RITC-labeled phage clone 15 were coinjected into Kras/p53$^{L/+}$, and tumor binding analyzed via intravital confocal microscopy.
(B) Unrelated phage clone was injected into Kras/p53$^{L/+}$ and analyzed via intravital confocal microscopy.
(C) Cy5.5-labeled phage clone 27 was injected into a wild-type mouse and analyzed via intravital confocal microscopy.

Found at doi:10.1371/journal.pmed.0050085.sg003 (1.4 MB TIF).

Acknowledgments

References

1. Li D, Xie K, Wolff R, Abbruzzese JL (2004) Pancreatic cancer. Lancet 363: 1049–1057.
2. Yeo CJ, Cameron JL, Maher MM, Sauter PK, Zahurak ML, et al. (1995) A prospective randomized trial of pancreaticogastrostomy versus pancreaticojejunostomy after pancreaticoduodenectomy. Ann Surg 222: 580–588; discussion 588–592.
3. Brentnall TA, Bronner MP, Byrd DR, Haggitt RC, Kimmey MB (1999) Early diagnosis and treatment of pancreatic dysplasia in patients with a family history of pancreatic cancer. Ann Intern Med 131: 247–255.
4. Canto MI, Goggins M, Yeo CJ, Griffin C, Axilbund JE, et al. (2004) Screening for pancreatic neoplasia in high-risk individuals: an EUS-based approach. Clin Gastroenterol Hepatol 2: 606–621.
5. Goggins M (2005) Molecular markers of early pancreatic cancer. J Clin Oncol 23: 4524–4531.
6. Pelaez-Luna M, Takahashi N, Fletcher JG, Chari ST (2007) Resectability of pre-symptomatic pancreatic cancer and its relationship with onset of diabetes: a retrospective review of CT scans and fasting glucose values prior to diagnosis. Am J Gastroenterol 102: 2157–2163.
7. Misek DE, Kuick R, Hanash SM, Logsdon CD (2005) Oligonucleotide-directed microarray gene profiling of pancreatic adenocarcinoma. Methods Mol Med 103: 175–187.
8. Bloomston M, Zhou JX, Rosemurgy AS, Frankel W, Muro-Cacho CA, et al. (2006) Fibrinogen gamma overexpression in pancreatic cancer identified by large-scale proteomic analysis of serum samples. Cancer Res 66: 2592–2599.
9. Yates JR 3rd, Eng JK, McCormack AL, Schieltz D (1995) Method to correlate tandem mass spectra of modified peptides to amino acid sequences in the protein database. Anal Chem 67: 1426–1436.
10. Joyce JA, Laakkonen P, Bernasconi M, Bergers G, Ruoslahti E, et al. (2003) Stage-specific vascular markers revealed by phage display in a mouse model of pancreatic islet tumorigenesis. Cancer Cell 4: 393–403.
11. Bardeesy N, Aguirre AJ, Chu GC, Cheng KH, Lopez LV, et al. (2006) Both p16(Ink4a) and the p19(Arf)-p53 pathway constrain progression of pancreatic adenocarcinoma in the mouse. Proc Natl Acad Sci U S A 103: 5947–5952.
12. Aguirre AJ, Bardeesy N, Sinha M, Lopez L, Tuveson DA, et al. (2003) Activated Kras and Ink4a/Arf deficiency cooperate to produce metastatic pancreatic ductal adenocarcinoma. Genes Dev 17: 3112–3126.
13. Hansel DE, Kern SE, Hruban RH (2003) Molecular pathogenesis of pancreatic cancer. Annu Rev Genomics Hum Genet 4: 237–256.
14. Schreiber FS, Deramaudt TB, Brunner TB, Boretti MI, Gooch KJ, et al. (2004) Successful growth and characterization of mouse pancreatic ductal cells: functional properties of the Ki-RAS(G12V) oncogene. Gastroenterology 127: 250–260.
15. Folli S, Westermann P, Braichotte D, Pelegrin A, Wagnieres G, et al. (1994) Antibody-indocyanin conjugates for immunophotodetection of human squamous cell carcinoma in nude mice. Cancer Res 54: 2643–2649.
16. Neri D, Carnemolla B, Nissim A, Leprini A, Querze G, et al. (1997) Targeting by affinity-matured recombinant antibody fragments of an angiogenesis associated fibronectin isoform. Nat Biotechnol 15: 1271–1275.
17. Kelly KA, Allport JR, Tsourkas A, Shinde-Patil VR, Josephson L, et al. (2005) Detection of vascular adhesion molecule-1 expression using a novel multimodal nanoparticle. Circ Res 96: 327–336.
18. Allport JR, Lim YC, Shipley JM, Senior RM, Shapiro SD, et al. (2002) Neutrophils from MMP-9- or neutrophil elastase-deficient mice show no defect in transendothelial migration under flow in vitro. J Leukoc Biol 71: 821–828.
19. Kelly KA, Jones DA (2003) Isolation of a colon tumor specific binding peptide using phage display selection. Neoplasia 5: 437–444.
20. Kelly KA, Clemons PA, Yu AM, Weissleder R (2006) High-throughput identification of phage-derived imaging agents. Mol Imaging 5: 24–30.
21. Kelly KA, Waterman P, Weissleder R (2006) In vivo imaging of molecularly targeted phage. Neoplasia 8: 1011–1018.
22. Montet X, Weissleder R, Josephson L (2006) Imaging pancreatic cancer with a peptide-nanoparticle conjugate targeted to normal pancreas. Bioconjug Chem 17: 905–911.
23. Reynolds F, Weissleder R, Josephson L (2005) Protamine as an efficient membrane-translocating peptide. Bioconjug Chem 16: 1240–1245.
24. Wunderbaldinger P, Josephson L, Weissleder R (2002) Crosslinked iron oxides (CLIO): a new platform for the development of targeted MR contrast agents. Acad Radiol 9 Suppl 2: S304–S306.
25. Schellenberger EA, Sosnovik D, Weissleder R, Josephson L (2004) Magneto/optical annexin V, a multimodal protein. Bioconjug Chem 15: 1062–1067.
26. Alencar H, King R, Funovics M, Stout C, Weissleder R, et al. (2005) A novel mouse model for segmental orthotopic colon cancer. Int J Cancer 117: 335–339.
27. Newton JR, Kelly KA, Mahmood U, Weissleder R, Deutscher SL (2006) In vivo selection of phage for the optical imaging of PC-3 human prostate carcinoma in mice. Neoplasia 8: 772–780.
28. Murtaugh LC, Leach SD (2007) A case of mistaken identity? Nonductal origins of pancreatic "ductal" cancers. Cancer Cell 11: 211–213.
29. Sonnenberg A, Liem RK (2007) Plakins in development and disease. Exp Cell Res 313: 2189–2203.

30. Weissleder R, Cheng HC, Bogdanova A, Bogdanov AJ (1997) Magnetically labeled cells can be detected by MR imaging. J Magn Reson Imaging 7: 258–263.

31. McBride G (2004) Screening methods may offer early diagnosis of pancreatic cancer. J Natl Cancer Inst 96: 1571.

32. Raymond K, Kreft M, Song JY, Janssen H, Sonnenberg A (2007) Dual role of alpha6beta4 integrin in epidermal tumor growth: tumor-suppressive versus tumor-promoting function. Mol Biol Cell 18: 4210–4221.

33. Aho S, Mahoney MG, Uitto J (1999) Plectin serves as an autoantigen in paraneoplastic pemphigus. J Invest Dermatol 113: 422–423.

34. Andra K, Nikolic B, Stocher M, Drenckhahn D, Wiche G (1998) Not just scaffolding: plectin regulates actin dynamics in cultured cells. Genes Dev 12: 3442–3451.

35. Osmanagic-Myers S, Wiche G (2004) Plectin-RACK1 (receptor for activated C kinase 1) scaffolding: a novel mechanism to regulate protein kinase C activity. J Biol Chem 279: 18701–18710.

36. Gregor M, Zeold A, Oehler S, Marobela KA, Fuchs P, et al. (2006) Plectin scaffolds recruit energy-controlling AMP-activated protein kinase (AMPK) in differentiated myofibres. J Cell Sci 119: 1864–1875.

37. Chari ST (2007) Detecting early pancreatic cancer: problems and prospects. Semin Oncol 34: 284–294.

38. Kim M, Gans JD, Nogueira C, Wang A, Paik JH, et al. (2006) Comparative oncogenomics identifies NEDD9 as a melanoma metastasis gene. Cell 125: 1269–1281.

39. Maser RS, Choudhury B, Campbell PJ, Feng B, Wong KK, et al. (2007) Chromosomally unstable mouse tumours have genomic alterations similar to diverse human cancers. Nature 447: 966–971.

Editors' Summary

Background. Pancreatic cancer is a leading cause of cancer-related death in the US. Like all cancers, it occurs when cells begin to grow uncontrollably and to move around the body (metastasize) because of changes (mutations) in their genes. If pancreatic cancer is found early, surgical removal of the tumor can sometimes provide a cure. Unfortunately, this cancer rarely causes any symptoms in its early stages and the symptoms it does eventually cause—jaundice, abdominal and back pain, and weight loss—are also seen in other illnesses. In addition, even though magnetic resonance imaging (MRI) or other noninvasive imaging techniques can be used to look at the pancreas, by the time tumors are large enough to show up on MRI scans, they have often already spread. Consequently, in most patients, pancreatic cancer is advanced by the time a diagnosis is made, hence surgery is no longer useful. These patients are given radiotherapy and chemotherapy but these treatments are rarely curative and most patients die within a year of diagnosis.

Why Was This Study Done? If more pancreatic cancers could be found before they had metastasized, it should extend the life expectancy of patients with this type of cancer. An early detection method would be particularly useful for monitoring people at high risk of developing pancreatic cancer. These include people with certain inherited cancer syndromes, pancreatitis (inflammation of the pancreas), and diabetes. Because cancer cells have many mutations, they express different proteins on their cell surface from normal cells. If these proteins could be identified, it might be possible to develop an "imaging probe"—a molecule that binds to a protein found only on cancer cells and that can be detected with MRI, for example—for early detection of pancreatic cancer. In this study, the researchers use a technique called "phage display" to identify several peptides (short sequences of amino acids, the constituent parts of proteins) that specifically bind to pancreatic cancer cells early in their development. They then investigate the possibility of developing an imaging probe from one of these peptides.

What Did the Researchers Do and Find? The researchers isolated early pancreatic cancer cells from a mouse model of human pancreatic ductal adenocarcinoma (PDAC; the commonest type of pancreatic cancer). Then, by mixing together these cells and normal mouse pancreatic cells with a library of phage clones (phages are viruses that infect bacteria; a clone is a group of genetically identical organisms), each engineered in the laboratory to express a random seven amino-acid peptide, they identified one clone, clone 27, that bound to the mouse tumor cells but not to normal cells. Clone 27 also showed up in the cancer cells in samples of mouse pancreatic intraepithelial neoplasias (PanINs; precursors to pancreatic cancer), mouse PDACs, and human PDACs.

The peptide in clone 27, the researchers report, binds to plectin-1, a protein present both inside and on the membrane of human and mouse PDAC cells but only on the inside of normal pancreatic cells. Finally, the researchers attached this plectin-1–targeted peptide (PTP) to a nanoparticles that was both magnetic and fluorescent (PTP-NP) and used special microscopy (which detects the fluorescent part of this very small particle) and MRI (which detects its magnetic portion) to show that this potential imaging probe was found in areas of PDAC (but not in normal pancreatic tissue) in the mouse model of human PDAC.

What Do These Findings Mean? These findings identify PTP as a peptide that can distinguish normal pancreatic cells from pancreatic cancer cells. The discovery that plectin-1 (a cytoskeletal component) is abnormally expressed on the cell surface of PDACs provides new information about the development of pancreatic cancer that could eventually lead to new ways to treat this disease. These findings also show that PTP can be used to generate a nanoparticle-based imaging agent that can detect PDAC within a normal pancreas. These results need to be confirmed in people—results obtained in mouse models do not always reflect what happens in people. Nevertheless, they suggest that PTP-NPs might allow the noninvasive detection of early tumors in people at high risk of developing pancreatic cancer, an advance that could extend their lives by identifying tumors earlier, when they can be removed surgically.

Additional Information. Please access these Web sites via the online version of this summary at http://dx.doi.org/10.1371/journal.pmed.0050085.

- The Panreatic Cancer Action Network and the Lustgarten Foundation for Pancreatic Cancer Research provide information, support, and advocacy for patients, families, and healthcare professionals
- The MedlinePlus Encyclopedia has a page on pancreatic cancer (in English and Spanish). Links to further information are provided by MedlinePlus
- The US National Cancer Institute has information about pancreatic cancer for patients and health professionals (in English and Spanish)
- The UK charity Cancerbackup also provides information for patients about pancreatic cancer